

Pulse Width Evolution in Gamma-Ray Bursts: Evidence for Internal Shocks

E. Ramirez-Ruiz^{1,2} and E. E. Fenimore¹

¹MS D436, Los Alamos National Laboratory, Los Alamos, NM 87545

²Institute of Astronomy, Madingley Road, Cambridge CB3 0HA UK

ABSTRACT

Many cosmological models of GRBs envision the energy source to be a cataclysmic stellar event leading to a relativistically expanding fireball. Particles are thought to be accelerated at shocks and produce nonthermal radiation. The highly variable temporal structure observed in most GRBs has significantly constrained models. By using different methods of statistical analysis in the time domain we find that the width of the large amplitude pulses in GRB time histories remains remarkably constant throughout the classic GRB phase. This is also true for small amplitude pulses. However, small and large pulses do not have the same pulse width within a single time history. We find a quantitative relationship between pulse amplitude and pulse width: the smaller amplitude peaks tend to be wider, with the pulse width following a power law with an index of ~ -2.8 . Internal shocks simulated by randomly selecting the Lorentz factor and energy per shell are consistent with a power law relationship. This is strong quantitative evidence that GRBs are indeed caused by internal shocks. The dependency of the width-vs.-intensity relationship on the maximum Lorentz factor provides a way to estimate that elusive parameter. Our observed power law index indicates that Γ_{\max} is $\lesssim 10^3$. We also interpret the narrowness of the pulse width distribution as indicating that the emission which occurs when one shell overtakes another is produced over a small range of distances from the central site.

Subject headings: gamma-rays: bursts - internal shocks

1. Introduction

The cosmological origin of GRBs, established as a result of optical follow-up observations of fading X-ray counterparts to GRBs (Costa, et al. 1997), requires an extraordinarily large amount of energy to flood the entire universe with gamma rays ($10^{52} - 10^{54}$ erg). The source of this energy is assumed to be a cataclysmic event (neutron star-neutron star merger, neutron star-black hole merger, or the formation of a black hole). The lack of apparent photon-photon attenuation of high energy photons implies substantial bulk relativistic motion. The relativistic shell must have a high Lorentz factor, $\Gamma = (1 - \beta^2)^{-1/2}$, on the order of 10^2 to 10^3 .

A growing consensus is that a central site releases energy in the form of a wind or multiple shells over a period of time commensurate with the observed duration of GRBs (Rees & Mészáros 1994). Each subpeak in the GRB is the result of a separate explosive event at the central site. General kinematic considerations impose constraints on the temporal structure produced when the energy of a relativistic shell is converted to radiation.

The purpose of this paper is to analyze the time histories of many GRBs to uncover the temporal evolution of the pulse width. In an earlier report (Ramirez-Ruiz & Fenimore 1999) we found no significant change in the average peak width in long bursts. Here, we analyze both long and short bursts in greater detail, as well as small and large amplitude pulses in individual bursts, and compare the results to internal shock models.

2. Observations

2.1. Temporal Evolution of the Average Pulse Width

Gamma-ray burst temporal profiles are enormously varied. Many bursts have a highly variable temporal profile with a time scale variability that is significantly shorter than the overall duration. Our aim is to characterize and measure the pulse shape as a function of arrival time. We will use the aligned peak method which measures the average pulse temporal structure by aligning the largest peak of each burst (Mitrofanov 1993).

The Burst and Transient Source Experiment (BATSE) catalog provides durations called T_{90} (Meegan et al. 1996), where T_{90} is the time which contains 90% of the counts. For the purpose of our analysis, we used two sets of bursts from the BATSE 4B Catalog that were brighter than 5 photons $\text{s}^{-1} \text{cm}^{-2}$ (256 ms peak flux measured in the 50-300 keV energy range) and with a 64ms temporal resolution. The first set used all 53 bursts that were longer than 20s, and the second set used all 23 bursts that were shorter than 20s. Each burst must have at least one peak, as determined by a peak-finding algorithm (similar to Li & Fenimore 1996), in each third of its duration. The largest peak in each third was normalized to unity and shifted in time, bringing the largest peaks of all bursts into common alignment. This method was applied in each third of the duration of the bursts. Thus, we obtained one averaged pulse shape, $I(t)$, for each third of the

bursts (as shown in Figure 1a for the long duration bursts and in Figure 1b for the short duration bursts). The average width is notably identical in each 1/3 of T_{90} in both long and short bursts. We estimate the differential spread, S , to be $\lesssim 1\%$ for the long duration bursts and $\lesssim 5\%$ for the short duration bursts.

The values $I(t)$ along the aligned timescale represent the average level of the emissivity of all contributing sources aligned at their primary peaks and thus the general character of the emission evolution of GRBs (see Mitrofanov 1993 for details). To resolve the true differences between the timescales in GRB pulses, one has to find the appropriate temporal correspondences in order to align the events, despite their probably different time histories. However, such a correspondence seems to exist because each burst has a specific moment, namely, the highest peak of the time history, which may be regarded as a physically unique reference moment. Furthermore, the highest peak is also where the highest signal-to-noise ratio is observed. The selection of a high brightness sample (5 photons $\text{s}^{-1} \text{cm}^{-2}$ in this case) is appropriate in order to avoid systematic effects that might change the observed time histories with different statistics. The time histories of dim events would be more randomized by fluctuations than the time histories of bright bursts. Using other GRB samples with a high signal-to-noise ratio ($\gtrsim 3$ photons $\text{s}^{-1} \text{cm}^{-2}$) gives similar results.

Figure 1 shows that the pulse width does not increase with time. It could be argued that the peak alignment method is uncertain because it only reflects the temporal evolution of the largest pulse width in the time histories. Thus, in the following section, we expand our analysis to individual pulses in GRB time histories.

2.2. Average Temporal Evolution of the Pulse Width

The substantial overlap of the temporal structures in the burst have made the study of individual pulses somewhat difficult. An excellent analysis has been provided by Norris, et al. 1996, who examined the temporal structure of bright GRBs by fitting time histories with pulses. The time histories were fit until all structure was accounted for within the statistics, thus, they effectively deconvolved the time history into all of the constituent pulses. From the set of pulses that they analyzed, we used the 28 bursts that have five or more fitted pulses (in the 55 keV - 115 keV BATSE channel) within their T_{90} duration. There was a total of 387 pulses in those 28 bursts. We obtain the Full Width Half Maximum (FWHM) from the pulse shape parameters found by Norris, et al. 1996. To find the average pulse width as a function of time, we first normalized the FWHM of each peak, within a burst, to the average FWHM of that burst. The purpose of such normalization is so that no one burst is allowed to dominate the pulse width average. Second, we normalized all the pulse amplitudes to the average amplitude. This is required in order to differentiate intrinsically large and small pulses in all bursts despite the total net counts. Figure 2 shows the average pulse width, $\frac{W}{\langle W \rangle}$, as a function of temporal position in the time history. The filled symbols give the average normalized width of the pulses that have a normalized amplitude, $\frac{A}{\langle A \rangle}$, greater than 1.0, while the open symbols show $\frac{W}{\langle W \rangle}$ for the pulses with a normalized

amplitude less than 1.0. Each group has about 180 pulses. The resulting average (in both samples) appears to be fairly constant in time. One cannot determine strict error bars because the uncertainties are not due to counting statistics (which, after all, are very good, since we are adding together ~ 180 pulses). Rather, the fluctuations are due to the way in which the various peaks add together. We used a linear fit to search for a trend. The resulting average temporal evolution of the pulse width is remarkably constant for both samples:

$$\begin{aligned} \frac{W}{\langle W \rangle} &= 0.82 - 0.01 \frac{T}{T_{90}} && \text{if } \frac{A}{\langle A \rangle} > 1.0 \\ &= 1.28 - 0.02 \frac{T}{T_{90}} && \text{if } \frac{A}{\langle A \rangle} < 1.0 . \end{aligned} \quad (1)$$

These curves are shown in Figure 2 as dotted lines.

A visual inspection of the pulses fitted to gamma ray bursts by Norris, et al. 1996 shows that the low amplitude pulses (in a single burst) tend to be wider although their shape may not be well determined. This is due to the fact that the actual temporal profile may contain “hidden” pulses which are not easy to deconvolve but contribute to the total emission. Furthermore, there are pulses that may overlap their neighbors and the pulse model is not sufficiently detailed to represent all of the individual emission events. Thus, larger pulses are much more successfully deconvolved than the smaller amplitude ones. It is more difficult to conclude that the average temporal evolution of the pulse width in small amplitude pulses is as constant over T_{90} as that of the large amplitude pulses for two reasons. First, the standard deviation of the distributions of pulse width values for small peaks is $\sim 1.7 - 2.2$ times greater than that found for the analysis of large amplitude pulses. Second, the linear correlation coefficient of the linear fit to the large amplitude pulses is ~ 1.12 times greater than the one found in the linear fit to the small amplitude pulses. Nevertheless, the small pulses show the same consistency in pulse widths as the large pulses.

This analysis of individual time histories agrees with what was found for the evolution of the average pulse structure for large peaks. Individual bursts show that larger peaks have about the same width at the beginning of the burst as near the end of the burst with a rather small variation. This is also true for smaller pulses. However, as we show in the next section, small and large pulses do not have the same pulse width within a single profile.

2.3. Pulse Width as a Function of Amplitude

GRBs are very diverse, with time histories ranging from as short as 50 ms to longer than 10^3 s. The long bursts often have very complex temporal structure with many subpeaks. The process that produces the peaks has a random nature, and the peaks that are produced vary substantially in amplitude. These pulses tend to be wider as their amplitudes decrease, within a single profile. To investigate the amplitude dependency of the pulse width, we used the 28 bursts described in

section 2.2. Each pulse (in each profile) was normalized to the average amplitude found in that burst. We selected four regions of normalized amplitudes: 0.1 - 0.3, 0.3 - 0.9, 0.9 - 1.5, 1.5 - 2.0. Each group has about 95 pulses. Figure 3 shows the aligned average pulse shape for the four ranges of normalized amplitudes. The pulse shape was calculated based on the general pulse shape proposed by Norris, et al. 1996:

$$\begin{aligned} I(t) &= A \exp\left[-\left(\frac{|t - t_{peak}|}{\sigma_r}\right)^\nu\right] & \text{if } t < t_{peak}, \\ &= A \exp\left[-\left(\frac{|t - t_{peak}|}{\sigma_d}\right)^\nu\right] & \text{if } t > t_{peak}, \end{aligned} \quad (2)$$

where t_{peak} is the time of the pulse’s maximum intensity (A); σ_r and σ_d are the rise and decay time constants, respectively; and ν is a measure of pulse sharpness, which Norris, et al. 1996 refer to as “peakedness”.

Each pulse, in each range of amplitude, was normalized to unity and then shifted in time, bringing the center of all pulses into common alignment. Note that the smaller peaks are wider than the larger peaks (see Fig. 3). We characterized the amplitude dependency of the pulse width in GRB time histories using the FWHM of the aligned average pulse shapes in Figure 3. The open diamonds in Figure 4 are the widths, W , of each aligned average pulse shape measured at the half maximum. We have fitted a power law and an exponential function to the points. The best-fit power law is $\frac{A}{\langle A \rangle} \sim [W_{FWHM}]^{-2.8}$ (The exponential fits had χ^2 values that were 1.4 times larger). The power-law function is shown in Figure 4 as a dotted line. This a robust result. Using the width at other values of the average pulse shape gives similar results. One thing that is not clear in our formulation is at what normalized amplitude to place the points. We have placed them at the mid-point of the selected amplitude ranges. If we were to use the average point of all the normalized amplitudes in each selected range, the result is still a power law: $\frac{A}{\langle A \rangle} \sim [W_{FWHM}]^{-3.0}$.

In summary, we find that the aligned average pulse shape can measure the amplitude dependency of the pulse width. The dependency is a power law in pulse width with an index that is between -2.8 and -3.0, depending on how it is measured.

Some limitations are necessarily inherent in our approach and selection of data. The conclusions we reach are based on measurements of a subset of the bursts detected by BATSE. We analyze the pulses deconvolved by Norris, et al. 1996 from a subset of relatively bright bursts with 64 ms temporal resolution. Analysis of pulses in shorter bursts using different data with much higher resolution will be the subject of another paper. In a multi-peaked event, all peaks would be seen if the burst is intense, whereas some peaks might be missed in a weak version of the event owing to the decrease of the signal-to-noise ratio. Moreover, smaller peaks of dimmer events might be missed owing to the absence of triggering of the instrument at those peaks. These effects might lead to a systematic decrease of the average number of peaks and/or to a decrease of estimated burst duration with decreasing burst intensity. Although our approach utilizes a sufficient number of pulses to represent adequately the temporal profile of a certain burst, our inferences concerning

pulse shape are drawn from those fitted pulses which do not overlap, as estimated by the relative amplitudes of two pulses and the intervening minimum. Several mutually reinforcing trends have been found by Norris, et al. 1996 in the analysis of the same sample. Thus, supporting the validity of our results.

From a phenomenological point of view, it has not been clear what the fundamental “event” in gamma-ray bursts is. The premise of our work has been that pulses are the basic unit in bursts. The relationship between pulse width and intensity supports this hypothesis. However, there may be other components in bursts, undefined by our approach, including long smooth structures at lower energies or very short spiky features at higher energies, which might represent distinct physical processes from the ones that are responsible for pulse emission. Evidence for a separate emission component, similar to those of the afterglows at lower energies, has been clearly found in some GRB light curves (Giblin, et al. 1999). These observations may indicate that some sources display a continued activity (at a variable level).

3. Pulses From Internal Shocks

Internal shocks occur when the relativistic ejecta from the central site are not moving uniformly. If some inner shell moves faster than an outer one ($\Gamma_i > \Gamma_j$) it will overtake the slower at a radius R_c . The two shells will merge to form a single one with a Lorentz factor Γ_{ij} . The emitted radiation from each collision will be observed as a single pulse in the time history (Piran & Sari 1997, Sari & Piran 1995). Several groups have modeled this process by randomly selecting the initial conditions at the central site (Kobayashi, Piran, & Sari 1997, Daigne & Mochkovitch 1998, Fenimore & Ramirez-Ruiz 1999). We will compare two aspects of these internal shock models to the pulse evolution studied in this paper: the trend for smaller pulses to be wider and the narrowness of the pulse width distribution.

3.1. Pulse Width vs. Intensity

We have simulated internal shocks as described in Fenimore & Ramirez-Ruiz 1999. In the notation of that paper, we have set the maximum initial energy per shell, E_{\max} , to be $10^{53.5}$ erg, the maximum thickness to be 0.2 lt-s, and the ambient density to be 1.0 cm^{-3} . We generated about 1.4 shells per s. Nine values of the maximum Lorentz factor, Γ_{\max} , were simulated from $10^{2.5}$ to $10^{4.5}$. The minimum Lorentz factor, Γ_{\min} , was 100. We took the resulting pulses and determined the peak intensity (assuming 0.064 s samples) and the FWHM. Figure 5a shows the distribution of pulse widths and intensities if Γ_{\max} is $10^{2.5}$ and 5b is for Γ_{\max} is $10^{4.5}$. The solid line is a power law with the index determined from the observations (i.e., from Fig. 4). Internal shocks show a trend that smaller pulses are wider. Indeed, one can estimate Γ_{\max} by measuring the index of the width vs. intensity distribution. By running models with a variety of values of

Γ_{\max} , we have found that the index is $\sim -5.25 + 0.975 \log_{10}(\Gamma_{\max})$. Our observed index of ~ -2.8 (from Fig. 4) indicates that Γ_{\max} is $\lesssim 10^3$.

3.2. Pulse Width as an indicator of R_c

A shell that coasts without emitting photons and then emits for a short period of time produces a pulse with a rise time related to the time the shell emits and a decay dominated by curvature effects (Fenimore, Madras, & Nayakshin (1996)). In the internal shock model, the shell emits for Δt_{cross} , where Δt_{cross} is the time it takes the reverse shock to cross the shell that is catching up. Following Kobayashi, Piran, & Sari 1997, $\Delta t_{\text{cross}} = l_j / (\beta_j - \beta_{rs})$, where l_j is the width of the rapid shell (β_j).

To calculate the observed pulse shape, one needs to combine Doppler beaming with the volume of material that can contribute at time T . Following Fenimore & Ramirez-Ruiz 1999 and Summer & Fenimore 1998, the resulting pulse shape is

$$\begin{aligned}
 V(T) &= 0 && \text{if } T < 0 \\
 &= \psi \frac{(R_c + 2\Gamma_{ij}^2 cT)^{\alpha+3} - R_c^{\alpha+3}}{(R_c + 2\Gamma_{ij}^2 cT)^{\alpha+1}} && \text{if } 0 < 2\Gamma_{ij}^2 T < \Delta t_{\text{cross}} \\
 &= \psi \frac{(R_c + \Delta t_{\text{cross}})^{\alpha+3} - R_c^{\alpha+3}}{(R_c + 2\Gamma_{ij}^2 cT)^{\alpha+1}} && \text{if } 2\Gamma_{ij}^2 T > \Delta t_{\text{cross}}
 \end{aligned} \tag{3}$$

where ψ is a constant, T is measured from the start of the pulse and α (~ 1.5) is the power-law index of the rest-frame photon number spectrum. The amplitude, ψ , depends on the amount of energy converted to gamma rays in a given collision.

Figure 6 shows the FWHM obtained from equation 3 (assuming that $l_j = 1$ light second and $\frac{\Gamma_i}{\Gamma_j} = 10$) as a function of the radius of emission, R_c , and the Lorentz factor of the resulting shell, Γ_{ij} . Note that a wide range of widths map into a narrow range of radii. In the internal shock scenario, the observed temporal structure reflects directly the activity of the inner engine. In Figure 7 we show the distribution of radii of emission using the FWHM calculated by equation 2 for the parameters provided by Norris, et al. 1996. The FWHM is used with Figure 6 to find a radius for each of the 387 pulses. The radius of emission is normalized by Γ_{ij}^2 , and, since the curves in Figure 6 are self-similar, all values of Γ_{ij} give the same distribution when divided by Γ_{ij}^2 . We define the radius spread, $\frac{\Delta R_c}{R_c}$, to be the ratio between the center and the standard deviation of the distribution of the radius of emission. This distribution shows that, if the spread of values of the Lorentz factors of the shells (Γ_{ij}) is small, the dynamical range of the radii of emission is also small: $\Delta R_c \sim 0.07 R_c$. The multiple-peaked time histories in the BATSE catalog reveal that the dynamical ranges in observed timescales within cosmic gamma-ray bursts (GRBs) are very large (see Norris, et al. 1996). For example, the total event durations range from 10 ms to 1000 s, with a dynamical range of almost 10^5 . Thus, the small variation in the values of the pulse width and radius spread parameter is remarkable.

In the internal shock scenario, the observed temporal structure reflects directly the activity of the inner engine. This engine must operate for a long duration, up to hundreds of seconds in some cases, and it must produce a highly variable wind to form shells that radiate. If the spread of values of the Lorentz factors (Γ_{ij}) is small, the range of radius is $\Delta R_c \sim 0.07 R_c$. The arrival time of the pulses at a detector such as BATSE has a one-to-one relationship with the time the shell was created at the central site. The time of arrival, T_{toa} , is $t_{ij} - R_c/c$ where t_{ij} is the time of the collision. But $t_{ij} - R_c/c$ is roughly t_{oi} , the time the shell was produced at the central site and is not dependent on other parameters such as R_c or the time of the collision (see, for example, Eq. 5 in Fenimore & Ramirez-Ruiz 1999). Thus, internal shocks also explain why the pulse width tends to be constant throughout the burst: the time of arrival in the time history is effectively just the time of generation of the pulses at the central site and is not related to the conditions or parameters of the collision.

4. Summary

We calculated the temporal evolution of the pulse width in gamma ray bursts. We found that the average aligned pulse width is a universal function that can measure the timescale of the largest pulses in the burst. For long and short bursts we found that the average aligned pulse width undergoes no significant change during the gamma-ray phase (see Fig. 1). The analysis of individual time histories agrees with what was found in the average aligned method. Individual bursts typically have no time evolution of the width of the largest pulses. This is also true for small pulses (see Fig. 2). However, in a time history, the smallest amplitude peaks tend to be wider (see Fig. 3). The dependency, as shown in Figure 4, is a power law in a amplitude with an index that is between -2.8 and -3.0, depending on how it is measured.

We have found that internal shocks can explain most of these characteristics. The time of arrival of a pulse is not related to the collision parameters so internal shocks can produce pulses that have the same characteristics at the beginning as at the end. Internal shocks produce pulses that are wider for smaller intensities. If the maximum Γ is $\lesssim 10^3$ the observed distribution (Fig. 4) is similar to the simulated distribution (Fig. 5). For such low values of Γ , deceleration is usually not important and the simulated time histories do not have pulses that get progressively wider (see Fenimore & Ramirez-Ruiz 1999). This is consistent with the analysis of this paper which did not find progressively wider pulses, although such pulses might have been missed because it is difficult to deconvolve many overlapping small pulses. Without substantial deceleration, the efficiency for converting bulk motion into radiation is $\lesssim 25\%$ (Fenimore & Ramirez-Ruiz 1999).

In the internal shock scenario, the temporal structure directly reflects the temporal behavior of the inner engine that drives the GRB. The pulse width gives information about the radius of colliding shells. Figure 6 shows that a wide range of widths maps into a narrow range of radii (see Fig. 7).

We thank Jay Norris for providing the pulse-fit parameters.

REFERENCES

- Costa, et al., 1997, *Nature*, 387, 783
- Daigne, F, & Mochkovitch, R., 1998, *MNRAS*, 296, 275
- Fenimore, E. E., Madras, C. D., & Nayakshin, S., 1996, *ApJ* 473, 998, astro-ph/9607163
- Fenimore, E. E. & Ramirez-Ruiz, E., 1999, submitted to *ApJ*, astro-ph/9909299.
- Giblin, T. W., et al., 1999, *ApJ* 524, L47
- Kobayashi, S., Piran, T., & Sari, R., 1997, *ApJ* 490, 92
- Li, H. & Fenimore, E. E., 1996, *ApJ* 469, L115
- Meegan, C. A., et al. 1996, *ApJS*, 106, 65
- Mészáros, P., & Rees, M. J., 1993, *ApJ*, 405, 278
- Mitrofanov, I. G., 1993, *AIP Conf. Proc.* 280, *Compton Gamma-Ray Observatory*, ed. M. Friedlander, N. Gehrels, & D. J. Macomb (New York:AIP), 761
- Norris, J. P., et al., 1996, *ApJ* 459, 393
- Piran, T., & Sari, R., 1997, *ApJ* 485, 270
- Ramirez-Ruiz, E., & Fenimore, E. E., 1999, *A&A Supplement*, *Proc. Of the Rome Conf. Gamma-Ray Bursts in the Afterglow Era*, in press, astro-ph/9812426
- Rees, M. J., & Mészáros, P., 1994, *ApJ*, 430, L93
- Sari, R., & Piran, T., 1995, *ApJ*, 455, L143
- Sari, R., & Piran, T., 1997, *ApJ*, 485, 270
- Summer, M. C., & Fenimore, E. E., *Gamma-Ray Bursts: 4-th Huntsville Symposium*, eds. Meegan, Preece, & Koshut, (*AIP Proc* 428) pg 765, astro-ph/9712302

Fig. 1.— Average peak alignment of gamma-ray emission from bright BATSE bursts. The largest peak in each third of the burst duration (i.e. T_{90}) is aligned and averaged. The three curves show the average pulse shape for the largest peak in the first third, second third, and last third of the bursts.

(a) Average pulse shape from 53 bright BATSE bursts with durations longer than 20 seconds. The difference in the average of the brightest pulse in each third is about 1%.

(b) Average pulse shape from 23 bright BATSE bursts with durations shorter than 20 seconds. The difference in the average of the brightest pulse in each third is less than 5%. We find a lack of temporal evolution of the width of the bright pulses over most of T_{90} . In addition, the average width is nearly identical in short and long bursts.

Fig. 2.— The evolution of pulse width with time. We sort the pulses into five time ranges spanning T_{90} . We further sort the pulses into bright peaks (amplitudes greater than the average for each burst, solid circles) and dim peaks (amplitudes less than the average, open triangles). Whereas Figure 1 is based on the brightest peaks, all 387 pulses from 28 bursts are included in this figure, divided roughly equally between bright and dim. For each group, we find the average of the observed width normalized to the average width for that burst ($A / \langle A \rangle$). The pattern that emerges is that both large and small peaks have remarkably constant widths throughout the duration of the bursts but the dim peaks tend to be wider than the bright peaks. The dotted lines are linear fits to the data and the slopes are less than 2%.

Fig. 3.— The average pulse profile as a function of relative intensity. We normalize the intensity of each peak to the average intensity of each burst. We then sort the 387 pulses from 28 bright bursts into four relative intensity ranges spanning from 0.1 to 2.0. For each group, we add the pulse shape Norris et al. (1996) found from deconvolving the burst time history into individual pulses. Thus, this could be considered an aligned-pulse test where every pulse is aligned rather than just the brightest peak. We do this for different relative intensities. There is a clear trend: the larger peaks tend to be narrower.

Fig. 4.— The intensity-width relationship. Short pulses are wider than large pulses. From Figure 3, the FWHM is a power law in intensity with an index about -2.8 (dotted line).

Fig. 5.— Pulse width vs. intensity from an internal shock model. Internal shocks are modeled as in Fenimore & Ramirez-Ruiz 1999 and the pulse width and intensity found for each pulse.

(a) Distribution if the maximum Lorentz factor is $10^{2.5}$. The solid line is the fit from Figure 4; that is, a power law slope of ~ -2.8 .

(a) Distribution if the maximum Lorentz factor is $10^{4.5}$. The distribution is quite different from the observations (solid line) implying that Γ_{\max} is not as large as $10^{4.5}$.

Fig. 6.— The expected pulse width as a function of the radius of colliding shells. Equation 3 is used to estimate the pulse width from the collision radius for various Lorentz factors ($l_j = 1$ light second and $\frac{\Gamma_i}{\Gamma_j} = 10$). Note that a wide range of widths maps into a narrow range of radii.

Fig. 7.— Distribution of collision radii based on observed pulse widths. Equation 3 is used to calculate R_c/Γ_{ij}^2 for 387 pulses from 28 bright bursts. The width of the distribution is remarkably narrow, $\sim 0.07\%$.

Figure 1a

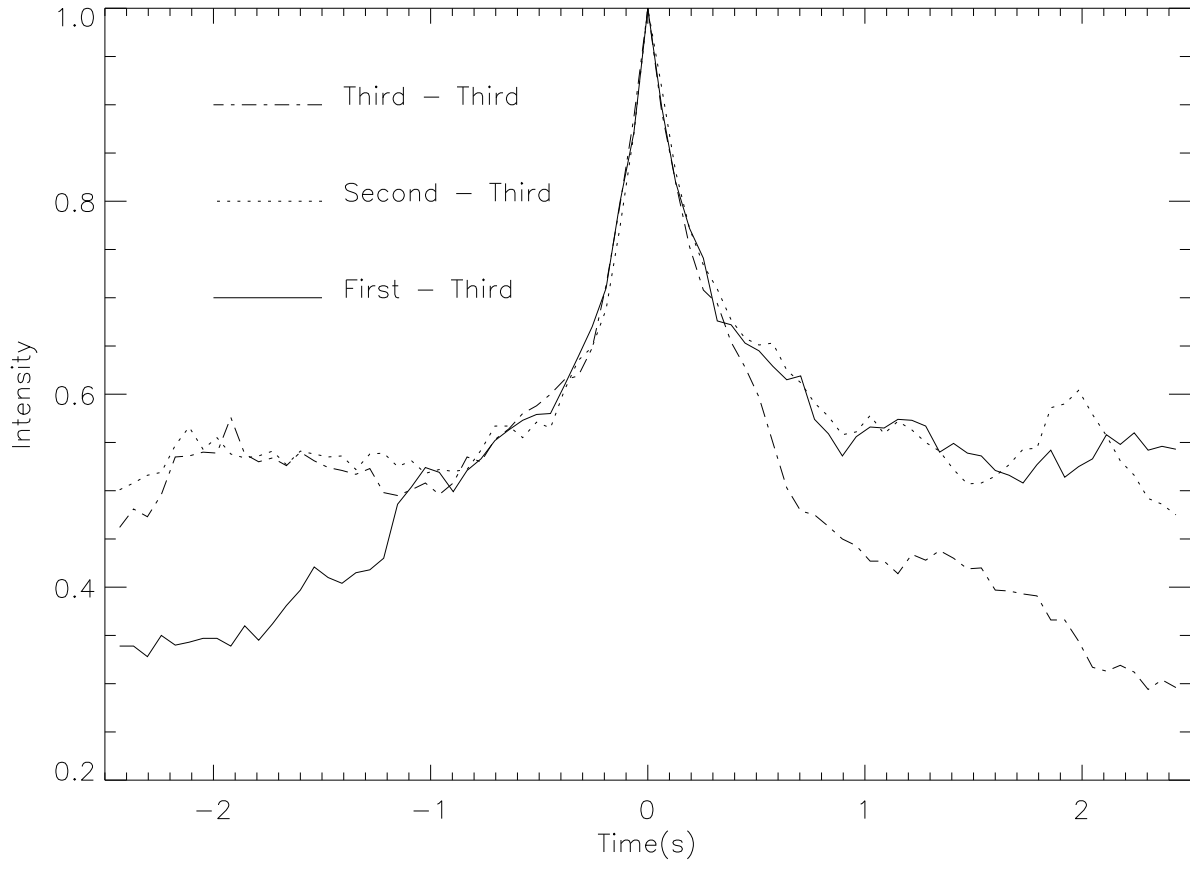


Figure 1b

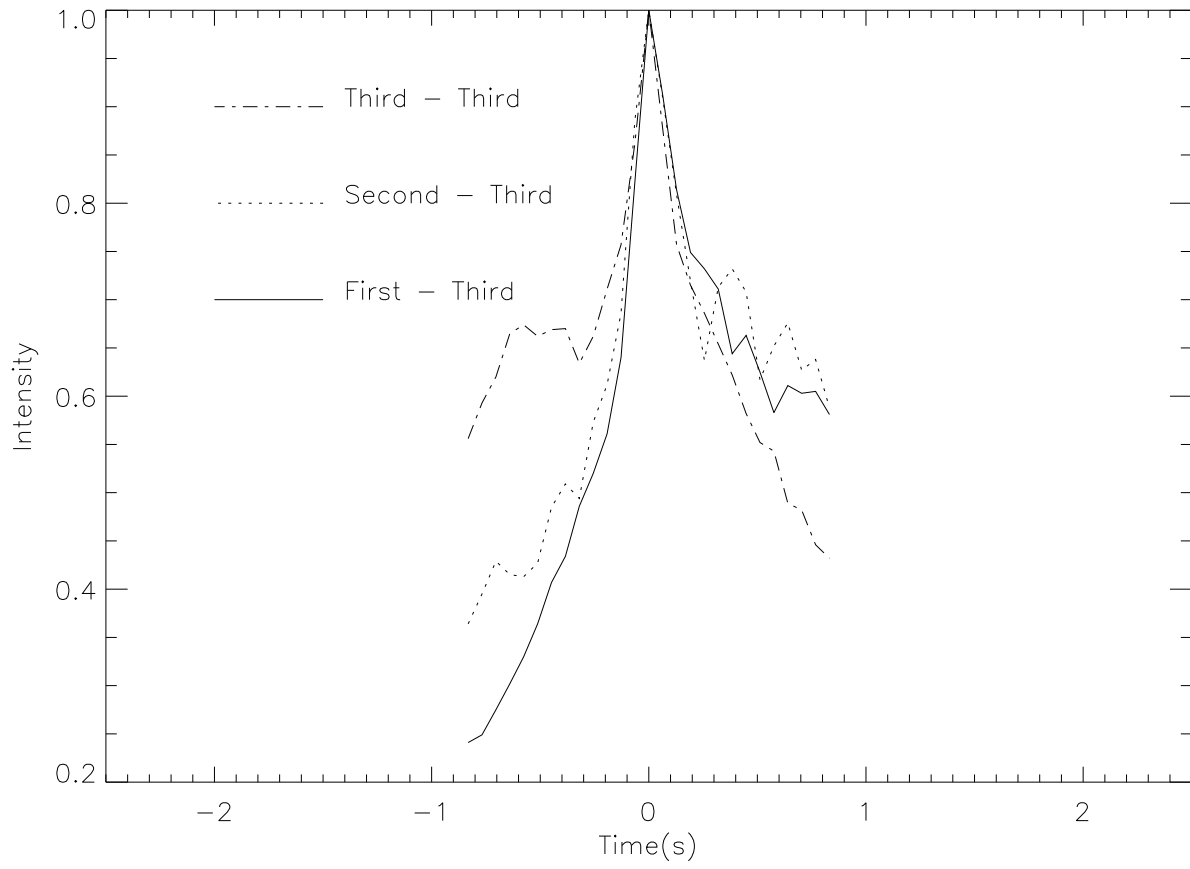


Figure 2

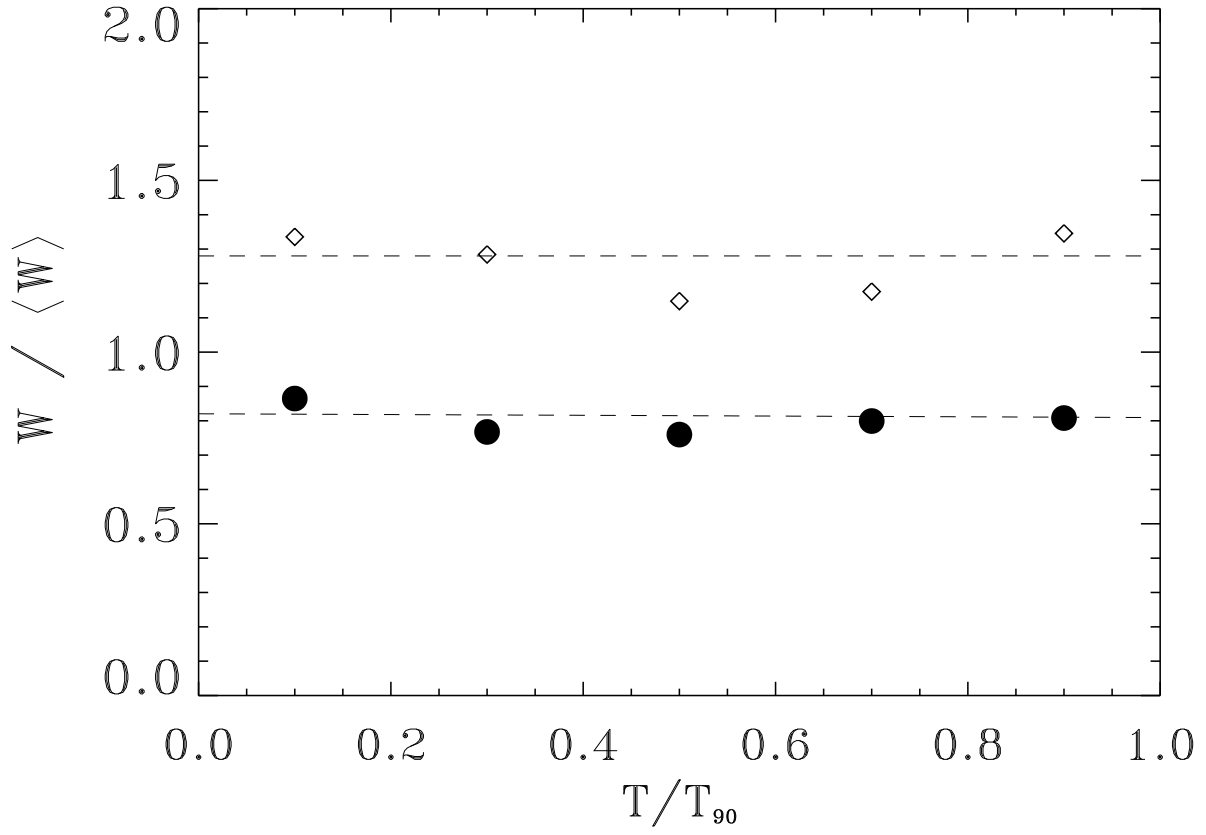


Figure 3

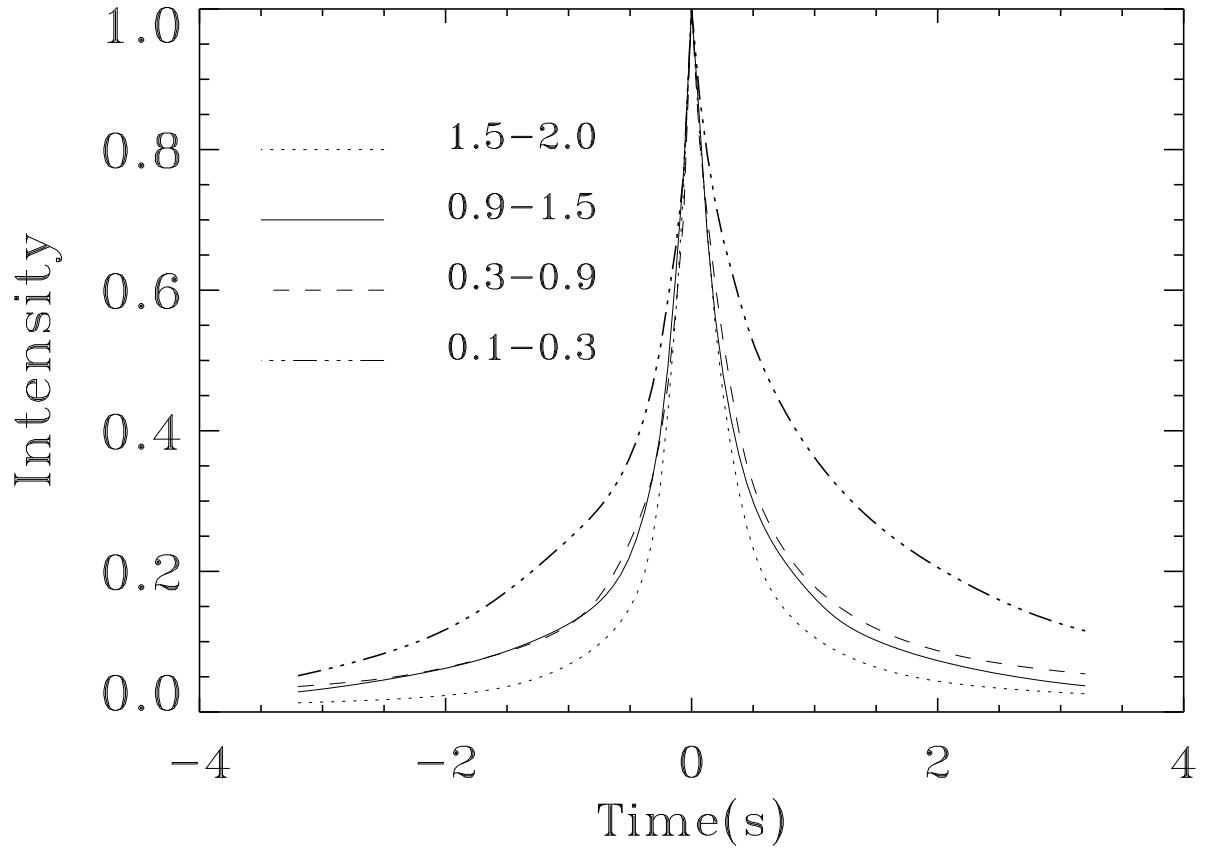


Figure 4

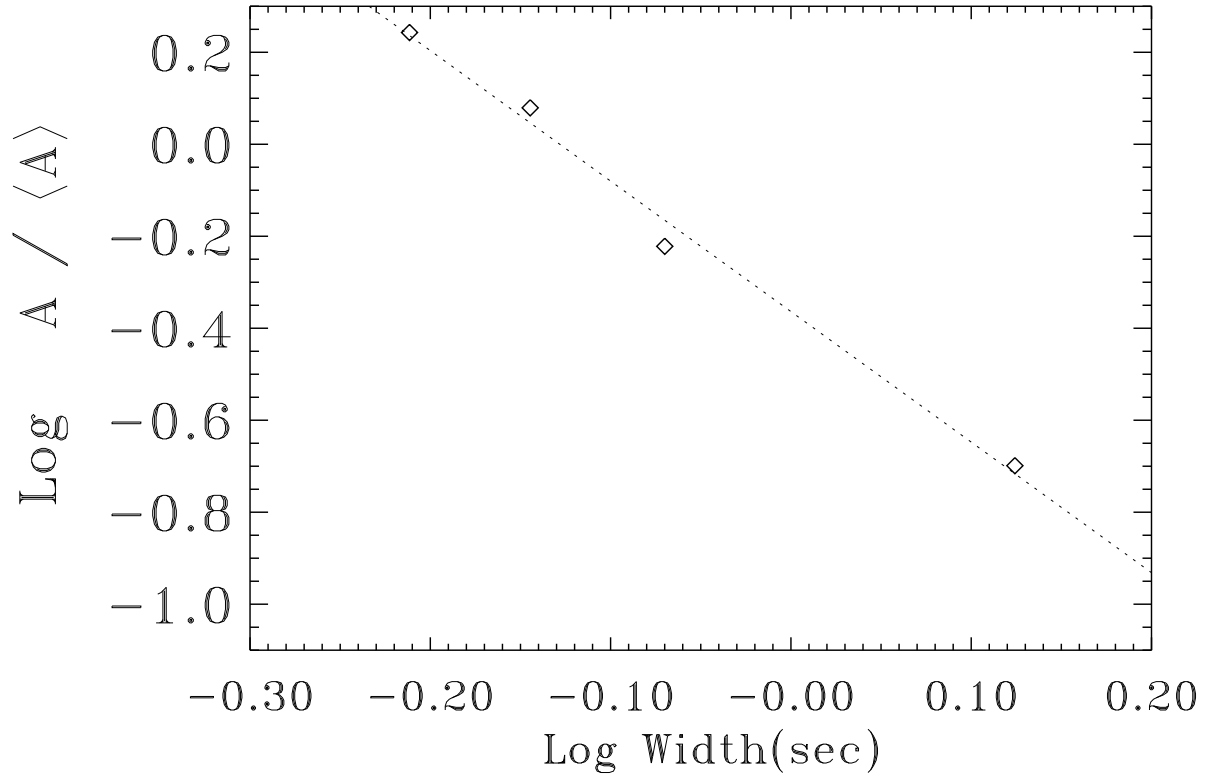


Figure 5a

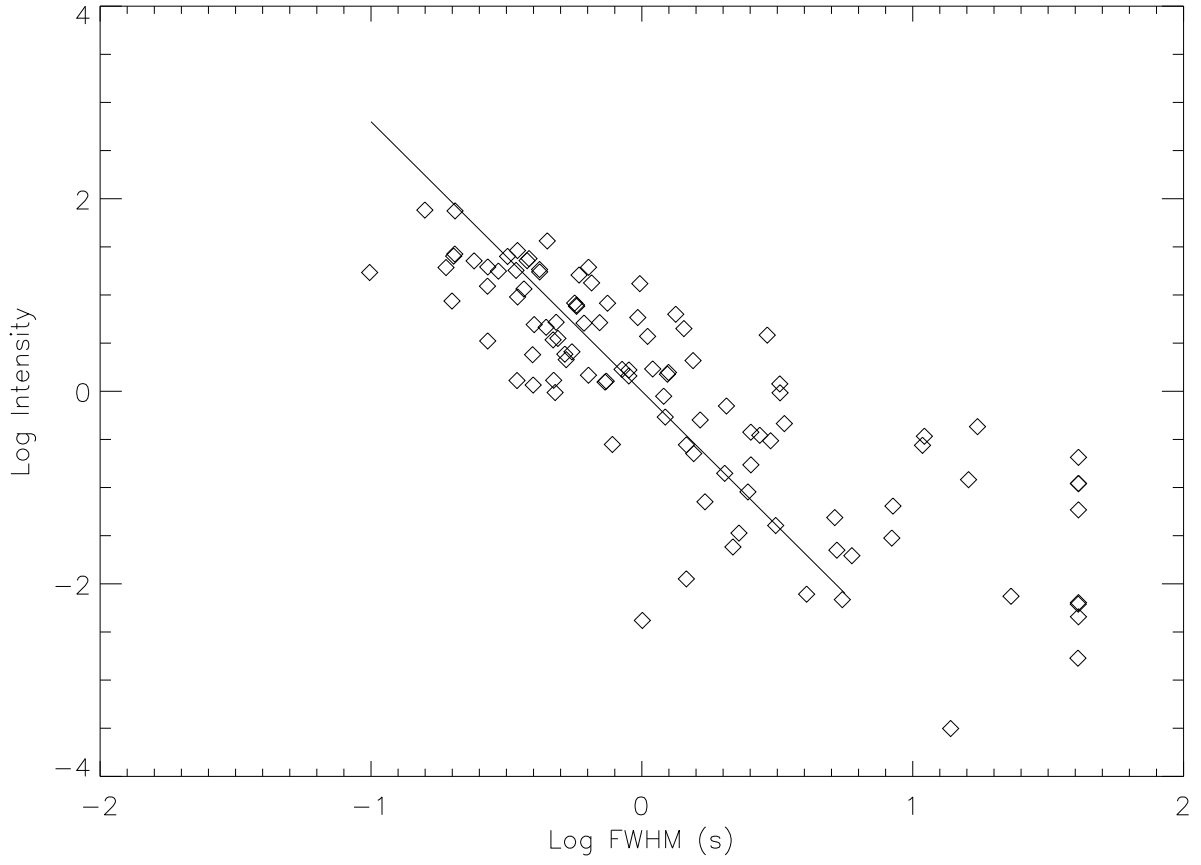


Figure 5b

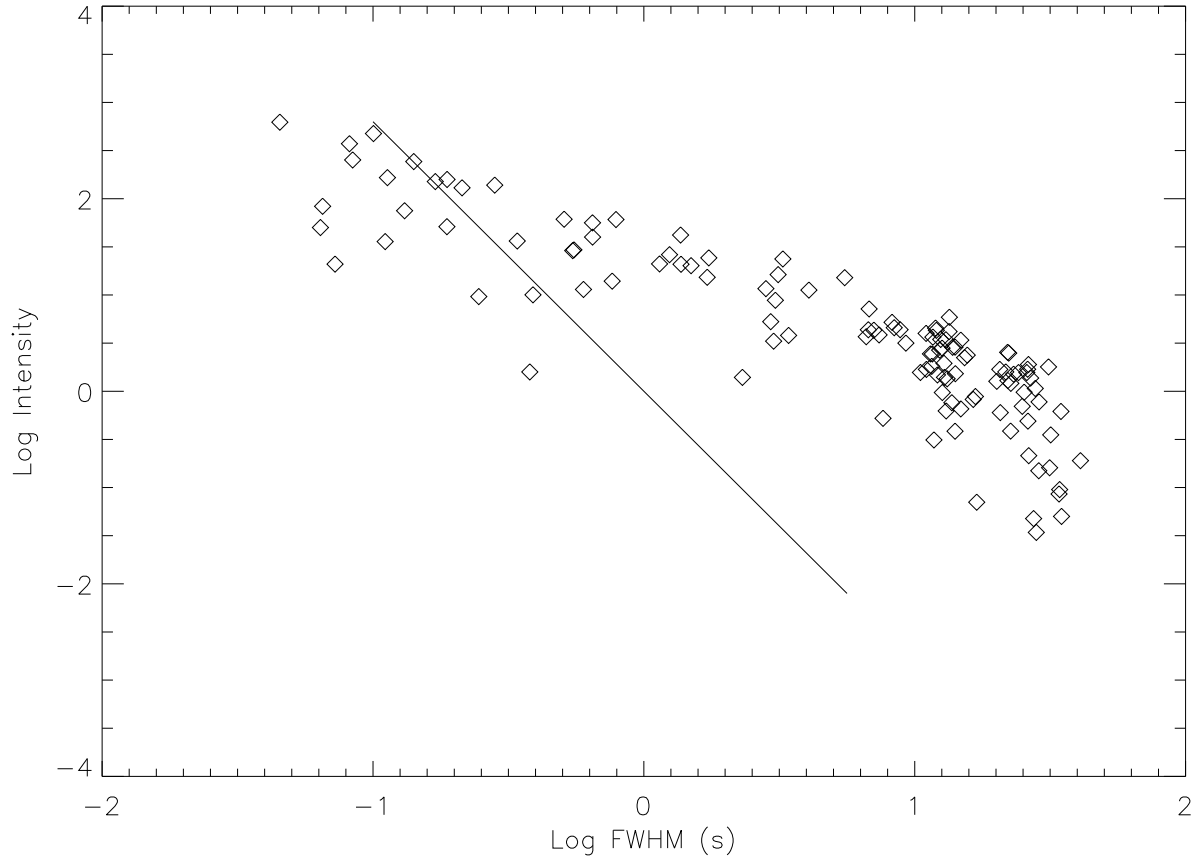


Figure 6

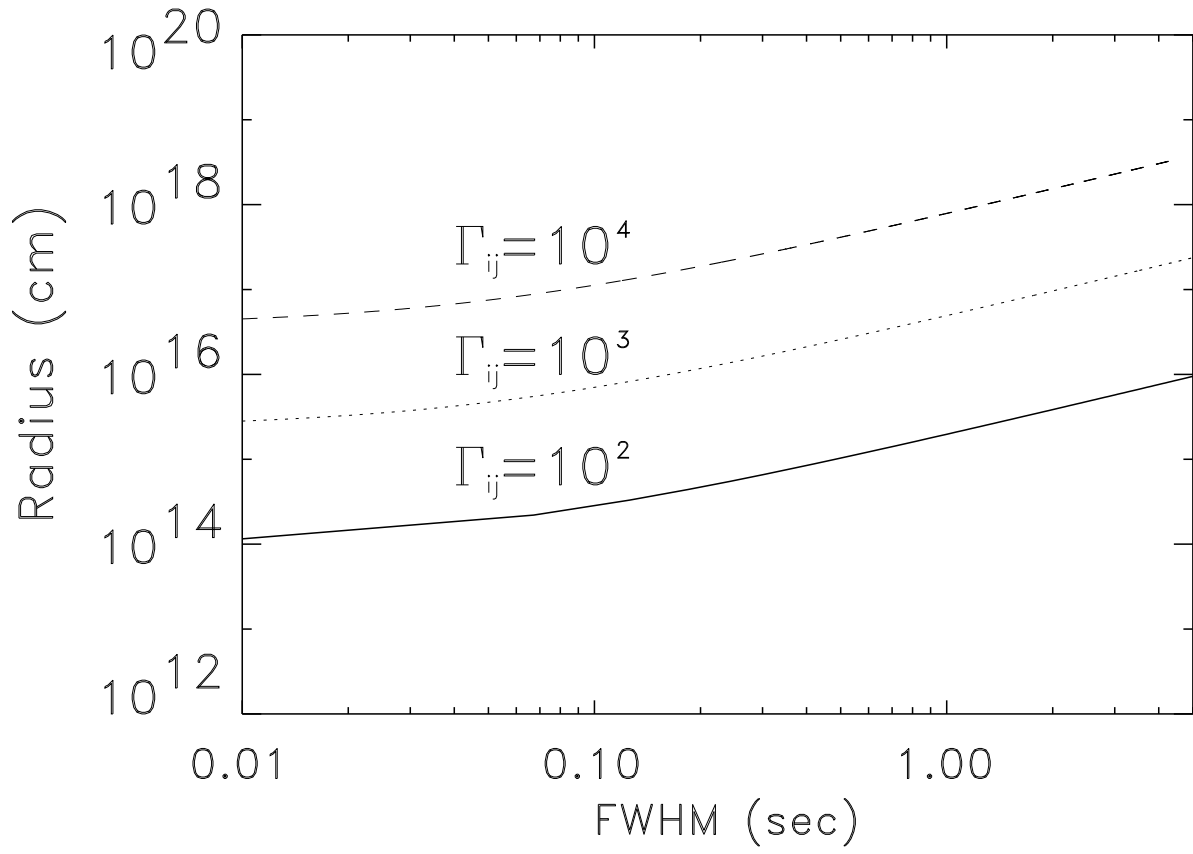


Figure 7

